Configurable Spin Orbital Interaction Utilizing Vector Beam Interference

Wei Liu, Zhen Chai, Kebin Shi, and Ze Zhang

***Abstract*—Spin-orbit interaction (SOI) of light has attracted enormous interest for its potential applications in controlling light at nanoscale and holds promise for future optical information technology and optoelectronics. In particular, the transverse spin in evanescent waves is regarded as distinct manifestation of SOI and an emerging candidate for miniaturizing optoelectronic circuits. However, further application has been hampered by the inability to conveniently generate light field with configurable transverse spin. Here, we present a simple method to generate free-space light field with arbitrary transverse spin utilizing vector beam interference and numerically demonstrate the configurable spin orbital coupling in nanophotonic waveguide. Chiral waveguide with excellent extinction ratio up to 42 dB is achieved in our simulation. The propagating direction of guided mode can be fully controlled via tuning the ellipticity of transverse spin. The device is compatible with existing integrated nanophotonic devices and may find valuable applications in future optical information processing and optical communication technology.**

***Index Terms*—Chiral waveguide, nanophotonics, spin orbit interaction, transverse spin, vector beam.**

I. Introduction

IT IS well known that light possess intrinsic spin angular momentum (SAM) and orbital angular momentum (OAM), as determined by the polarization and spatial degrees of the freedom of light [1], [2], [3], [4], [5], [6]. In traditional macroscopic geometrical optics, these two degrees of freedom are usually manipulated independently and the SOI phenomena can be neglected. However, the SOI must be considered in modern optics dealing with nonparaxial structured light field with sub-wavelength inhomogeneities [7], [8], [9], [10]. In particular, the spin and orbital angular momentum become tightly coupled with each other in strongly nonparaxial regime such as nanophotonics, near-field optics and plasmonics [11], [12], [13], [14]. The studies of optical SOI recently have revealed that the spatial degrees of freedom can be affected or controlled by spin of light via SOI phenomena [15], [16], [17]. These extraordinary characteristics of SOI can find applications in optical diodes, chiral photonics, optical communications, metrology and quantum information processing.

The simplest example of an optical field carrying SAM is an elliptically polarized plane wave, whose spin is proportional to the polarization helicity and collinear with the wave vector. Therefore, the spin of this kind of elliptically polarized light field is also called longitudinal spin. In recent years, there has been increasing interest in the transverse SAM of light in the study of SOI. Transverse spin is widely found in strongly nonparaxial regime, where the longitudinal field components emerge due to the transversality of light [18], [19], [20]. Studies have revealed the transverse spin in evanescent waves originates from the SOI in laterally confined propagating modes [21], [22]. In sharp contrast with the normal longitudinal spin, transverse spin has a spin axis orthogonal to the propagating direction of light. More interestingly, the rotation of transverse spin can play a key role in the process of SOI associated with near-field optics and is directly linked to the propagating direction of evanescent wave [23], [24]. Such intriguing physics effects of transverse spin provides possibility for realizing controllable spin-direction coupling between free space light field and guided mode of nanoscale waveguide [11], [25], [26], [27], [28]. The direction of transverse spin for evanescent wave of transverse electric (TE) mode is perpendicular to the substrate, which exactly matches the spin of normally incident light with circular polarization. Therefore, previous researches on spin controlled chiral waveguide mostly focused on coupling chiral TE mode for the convenience to generate and modulate circularly polarized light [11], [26], [29]. However, due to the lack of fast and tunable methods of generating light field with configurable transverse spin, only a few studies on coupling chiral of transverse magnetic (TM) mode of waveguide require complicated design of nano structures and oblique illumination [25], [26], [30]. As the evanescent field of TM mode is located near the top surface of the waveguide, it has significant advantages over TE mode in applications such as on-chip sensors, interlayer coupling of 3D waveguide [36]. In order to expand the application scope of SOI, numerous significant works have been performed to investigate the method of generating light field with tunable transverse spin over the past few years. However, those methods require complex optical design and expensive phase modulation equipment, and the switching speed of spin direction

Manuscript received 14 November 2022; revised 23 December 2022; accepted 27 December 2022. Date of publication 30 December 2022; date of current version 6 January 2023. This work was supported in part by the National Natural Science Foundation of China under Grants 12074350 and 62105341 and in part by the Natural Science Foundation of Shandong Province under Grant ZR2021QF126. *(Corresponding author: Wei Liu.)*

Wei Liu is with the Aerospace Information Research Institute, Chinese Academy of Sciences, Beijing 100094, China (e-mail: liuwei02@aircas.ac.cn).

Zhen Chai is with the Beihang University, Beijing 100191, China (e-mail: zhenchai@buaa.edu.cn).

Kebin Shi is with the Peking University, Beijing 100871, China (e-mail: kebinshi@pku.edu.cn).

Ze Zhang is with the Qilu Aerospace Information Research Institute, Shandong 250101, China (e-mail: zhangze@aircas.ac.cn).

Digital Object Identifier 10.1109/JPHOT.2022.3233071

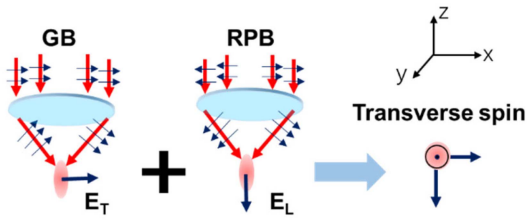

Fig. 1. The basic principle for synthesizing light field with transverse spin. GB: Gaussian beam, RPB: radially polarized beam, $\boldsymbol{E}_T$: transverse electric field component, $\boldsymbol{E}_L$: longitudinal electric field component.

cannot meet the application requirements of highspeed optical information processing and communication. Developing a robust and cheap method to generate light field with tunable transverse spin remains a great challenge in optoelectronic circuits [31], [32], [33], [34], [35].

In this work, we propose a simple scheme to generate arbitrary transverse spin in free-space light field utilizing vector beam interference and numerically demonstrate a configurable spin orbital coupling device with high extinction ratio in nanophotonic waveguide. The longitudinal field component is generated by a tightly focused radially polarized beam, while the transverse field component is provided by another Gaussian beam. When two beams interference at the focus and maintain $\pi/2$ phase difference with respect to each other, the electric vector of total field will rotate in plane parallel to the path of light beam. In this way, free space light field with transverse spin is generated and can be rapidly tuned by changing the amplitude and phase of two beams. A gold nanoparticle as polarization maintaining scatterer is placed on the surface of nanophotonic waveguide to couple excitation light into eigenmode of waveguide through the evanescent wave. In contrast with other sophisticated chiral photonic devices, our proposed device is perfectly symmetric and simple, which only consists of a nanoparticle located on the top of waveguide. The unidirectionality can be optimized and fully controlled by modulating the phase and amplitude of two coherent vector beams. Such spin orbital coupling method provides a unique way for designing chiral nanophotonic devices and could find direct applications in integrated ellipsometry and quantum processing and topological photonics.

II. Theoretical Model

A. Basic Principle for Generating Light Field With Transverse Spin

The proposed scheme of generating free space light field with transverse spin is sketched in Fig. 1. The key to generate transverse spin with arbitrary ellipticity is to create a longitudinal field component and another mutually orthogonal transverse field component for which the amplitude and phase can be tuned independently. When a vector beam is tightly focused, the radial component of the incident beam contributes to the transverse and longitudinal field components near the focal plane, while the azimuthal component in the incident beam just contributes to the transverse field component on the focal plane. If a vector light beam with symmetric polarized field components is focused using a high numerical-aperture (NA) objective, the transverse component will be destructed and only longitudinal field component left at the center of focus. Based on the above discussion, robust longitudinal field component can be developed with a tightly focused radially polarized beam whose polarization distribution is perfectly centrosymmetric. The transverse field component is provided by another independent Gaussian beam focused by the same objective. Transverse spin with arbitrary ellipticity can be generated by just tuning the amplitude and phase difference of two incident beams. When the two orthogonal field components have same amplitude and phase difference of $\pm\pi/2$ in focal volume, transverse spin with perfect circular polarization can be obtained.

According to the Richards-Wolf vectorial diffraction theory, the electric field of a tightly focused radially polarized beam ERP are given on the form:

$$\mathrm{E}_{RP}(\rho,\varphi,z)=\frac{ikf^2}{2\omega_0}\sqrt{\frac{n_1}{n_2}}E_0e^{-ikf}\begin{bmatrix} iI_1\cos\varphi \\ iI_1\sin\varphi \\ -4I_2 \end{bmatrix}d\theta \quad (1)$$

And the electric field of a Gaussian beam with polarization along x direction $\boldsymbol{E}_{LP}$ are given as:

$$\mathrm{E}_{LP}(\rho,\varphi,\mathrm{z})=\frac{ikf}{2}\sqrt{\frac{n_1}{n_2}}E_0e^{-ikf}\begin{bmatrix} I_3+I_4\cos 2\varphi \\ I_4\sin 2\varphi \\ -2iI_5\cos\varphi \end{bmatrix} \quad (2)$$

where ρ, φ and z are unit coordinate vectors in cylindrical coordinate system, E_0 is initial amplitude of radial polarized beam and linearly polarized beam separately. k is the wave vector of incident beam, f is the focus length of objective, ω_0 denotes the beam waist radius, n_1 and n_2 are the refractive index before and after the objective respectively. θ is the divergence angle of the focused beam and I_n are abbreviations for integral functions of Bessel function with the following expressions:

$$\begin{aligned}
I_1 &= \int_0^{\theta_{max}} f_w(\theta)(\cos\theta)^{\frac{3}{2}}\sin^2\theta \\
&\quad\times J_1(k\rho\sin\theta)e^{ikz\cos\theta}\,d\theta \\
I_2 &= \int_0^{\theta_{max}} f_w(\theta)(\cos\theta)^{\frac{1}{2}}\sin^3\theta \\
&\quad\times J_0(k\rho\sin\theta)e^{ikz\cos\theta}\,d\theta \\
I_3 &= \int_0^{\theta_{max}} f_w(\theta)(\cos\theta)^{\frac{1}{2}}\sin\theta(1+\cos\theta) \\
&\quad\times J_0(k\rho\sin\theta)e^{ikz\cos\theta}\,d\theta \\
I_4 &= \int_0^{\theta_{max}} f_w(\theta)(\cos\theta)^{\frac{1}{2}}\sin\theta(1-\cos\theta) \\
&\quad\times J_2(k\rho\sin\theta)e^{ikz\cos\theta}d\theta \\
I_5 &= \int_0^{\theta_{max}} f_w(\theta)(\cos\theta)^{\frac{1}{2}}\sin^2\theta \\
&\quad\times J_1(k\rho\sin\theta)e^{ikz\cos\theta}\,d\theta
\end{aligned} \quad (3)$$

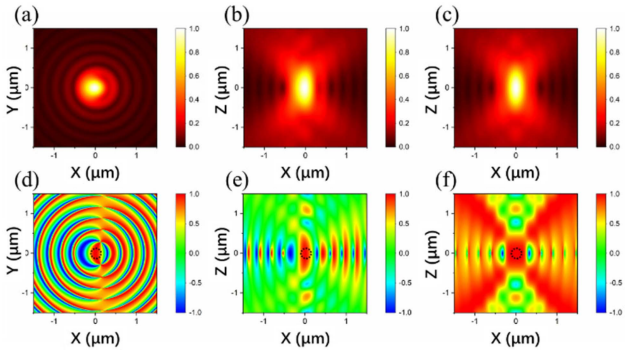

Fig. 2. The simulation result of the generated light field with transverse spin. (a)–(c) The electric field amplitude distribution of the total light field in x-y, x-z and y-z planes cross the focus. (d)–(f) The spin density distribution calculated by $\boldsymbol{E}x$ and $\boldsymbol{E}z$ component in x-y, x-z and y-z planes cross the focus.

Where J_n is the nth-order Bessel function. the function $f_w(\theta)$ is given by: $f_w(\theta) = \exp(-\sin^2\theta/\mathrm{f_0}^2\sin^2\theta_{\max})$. Here, the f_0 is the filling factor of the objective. The interference electric field $\boldsymbol{E} = \boldsymbol{E}_{RP}+\eta exp(i\varphi_0)\boldsymbol{E}_{LP}$ can be calculated with (1) and (2), here the η and φ_0 are the additional amplitude and phase modulation factor. The transverse field component $\boldsymbol{E}_x$ and longitudinal field component $\boldsymbol{E}_z$ of total electric field are obtained after transforming the cylindrical coordinate to Cartesian coordinates. After the phase difference and the amplitude ratio are set to $[\varphi_{Ez\text{-}Ex}, |\boldsymbol{E}_z|/|\boldsymbol{E}_x|] = [\pm 0.5\pi, 1]$ by tuning the parameters φ_0 and η at the center of focus, free space light field with perfect transverse spin can be generated.

The normalized spin density σ derived from equation of polarization ellipse was utilized to describe the ellipticity of polarization for the transverse spin [36], which can be expressed as:

$$\sigma = \frac{2E_z E_x sin\delta}{E_z^2 + E_x^2} \tag{4}$$

where δ is the phase difference between two electric components.

Based on the theoretical models above, the amplitude distribution and spin characteristics of the light field generated by vector beam Interference can be analyzed. The linearly polarized beam with polarization along the x direction is superimposed with another radially polarized beam coaxially in our simulation. Two beams with the same wavelength of 532 nm and waist diameter of 6 mm are tightly focused by an objective with NA of 0.95 and propagating along z direction in the defined coordinates. Fig. 2(a)-(c) shows the simulated total electric field distribution in three orthogonal planes in the confocal region when incident beams are configured to satisfied the conditions of $[\varphi_{Ez\text{-}Ex}, |\boldsymbol{E}_z|/|\boldsymbol{E}_x|] = [0.5\pi, 1]$. As depicted in Fig. 2, the main lobe of focal spot is asymmetric due to the interference of radial and linearly polarized beam. Due to the spin density σ relays on the electric field components $\boldsymbol{E}_x$ and $\boldsymbol{E}_z$, the calculated spin density distribution also shows uniformity induced by the asymmetric of electric field in x direction. As uniformity is crucial for many practical applications, the effective volume with high and uniform spin density need to be located. A spherical volume with spin density above 0.85 was marked in Fig. 2(d)-(f) by a dash circle with diameter of 250 nm. To take fully advantage of the effective spherical light field volume in applications involving nanoantenna coupling, the size of coupling antenna should be compactly designed and precisely align with the focus of light field.

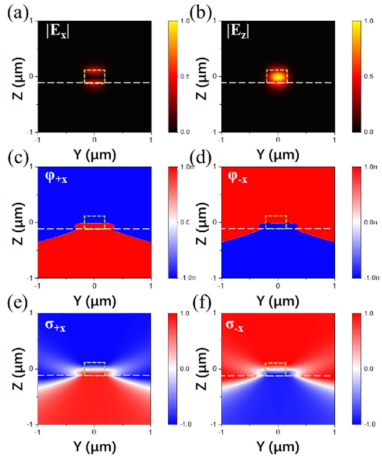

Fig. 3. The simulated light field distribution for TM mode on the cross section of the single mode Si_3N_4 waveguide on silica substrate. (a) and (b) The light field amplitude distribution of $\boldsymbol{E}_x$ and $\boldsymbol{E}_z$ components for TM mode of the waveguide respectively. (c) and (d) The phase difference between $\boldsymbol{E}_x$ and $\boldsymbol{E}_z$ components of TM mode propagating along +x and -x directions respectively. (e) and (f) The helicity distribution of polarization for the TM mode of waveguide as a guided TM mode propagating along the +x and -x directions respectively.

B. TM Mode Characteristics of a Single Mode Waveguide

To validate the spin characteristics of guided mode in nanoscale waveguide, the eigen TM mode of a Si3N4 single mode waveguide was simulated utilizing the finite-different time domain (FDTD) method. The width and thickness of the Si3N4 waveguide on SiO2 substrate in our simulations are set to 250 nm and 220 nm which are chosen via mode analysis in the planer slab nano-waveguide to ensure no high-order guided mode allowed. The electric field distributions of $\boldsymbol{E}_z$ and $\boldsymbol{E}_x$ for the eigen TM mode are shown in Fig. 3(a) and (b) respectively. The phase difference of $\boldsymbol{E}_x$ and $\boldsymbol{E}_z$ components of the eigen TM mode are shown in Fig. 3(c)-(f). It can be seen that the phase difference between $\boldsymbol{E}_x$ and $\boldsymbol{E}_z$ has opposite signs for upper and under surfaces of the waveguide, and the absolute value of the phase difference is strictly equal to 0.5π near the surface of waveguide. The value of spin density on the cross section of waveguide is calculated utilizing (4) and shown in Fig. 3(e) and (f). The absolute value of spin density is 0.98 and its inhomogeneity is less than 0.01 within height of one wavelength above the upper surface of waveguide. The simulations above clearly prove that the propagating direction of TM mode is strictly bounded with spin density of evanescent wave.

C. Chiral Characteristics of The Proposed Spin Orbit Interaction Method

The scheme of the proposed spin orbit interaction method is shown in Fig. 4(a). A linearly polarized beam and another

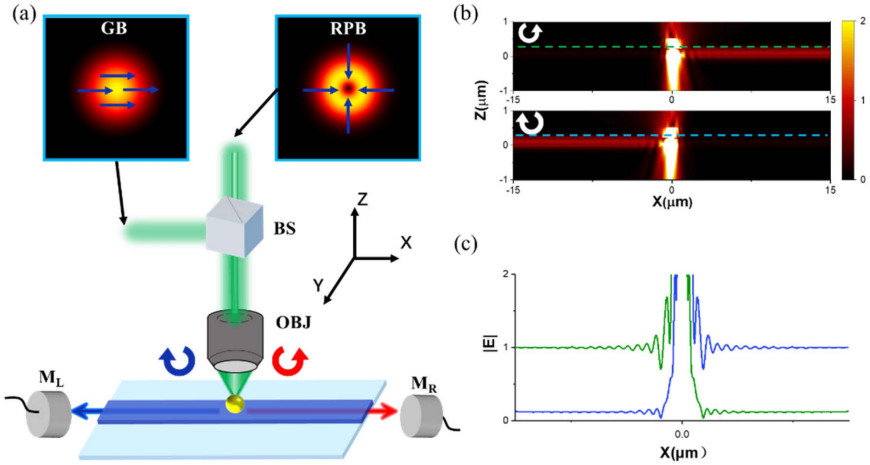

Fig. 4. The scheme of the proposed spin orbit interaction method and the distribution of electric field amplitude of chiral waveguide. (a) The scheme of the proposed spin orbit interaction. (b) The amplitude distribution of electric field in the x-z plane passing through the central axis of waveguide illuminated by light field with clockwise and anticlockwise transverse spin respectively. (c) The electric field amplitude profile performed along the dash lines of (b) which placed 10 nm above the upper surface of waveguide. BS: beam splitter, OBJ: objective, M_L and M_R: energy monitors.

radically polarized beam are combined by a non-polarizing beam splitter and then focused by a high NA objective to generate light field with independent longitude and transverse electric field components. The spin density can be tuned arbitrarily by modulating the phase and amplitude of the Gaussian beam. Free-space light field with circular transverse spin is obtained in the focal volume when the phase difference and amplitude ratio are exactly set to $\pm\pi/2$ and 1. A gold particle is chosen as antenna to couple light into the guided mode of waveguide. Comparing with antenna made of all-dielectric structure, the gold nanoparticle with high scattering cross section can couple light into waveguide more effectively due to its surface plasmon resonance in visible band [37]. As the direction of transverse spin for evanescent wave is uniquely locked with the direction of propagation, the propagating direction of excited mode in waveguide is determined by the spin direction of incident electric field. We calculated the scattering cross section of gold particles with different diameters at wavelength of 532 nm. The gold nanoparticle with diameter of 90 nm has the largest scattering cross section at wavelength 532 nm, which helps to achieve the largest coupling efficiency of the transverse spin based chiral device.

Fig. 4(b) shows the amplitude distribution of electric field along the transverse xz-plane passing through the central axis of waveguide for incident field with anticlockwise and clockwise circular transverse spin, respectively. To clearly show the difference between the left and right arms, the electric field was normalized by the maximum amplitude at the output ports of the two arms in Fig. 4(b). We clearly see that light is coupled to the right arm of the waveguide (left arm, respectively) for incident light field with anticlockwise (clockwise, respectively) circular transverse spin. In Fig. 4(c) are the amplitude profiles of electric field along the green and blue dashed lines of Fig. 4(b), in which the maximum amplitude of electric field at the excited arm is about 7.5 times larger than the other arm. In order to quantitatively evaluate the performance of chirality of the spin-dependent waveguide, extinction ratio is utilized to characterize the performance of the coupler. The extinction ratio $\boldsymbol{ER}$ is calculated using the photon fluxes at both outputs of the waveguide, which is expressed as the form of $\boldsymbol{ER} = 10\lg(\boldsymbol{T}_L/\boldsymbol{T}_R)$, where $\boldsymbol{T}_L$ and $\boldsymbol{T}_R$ are photon fluxes from the left and right arm of the waveguide respectively. With the definition of extinction ratio, the extinction ratio of our designed chiral waveguide can be calculated by the energy output recorded by the energy monitor M1 and M2 in Fig. 4(a), which is 17.5 dB at wavelength of 532 nm in simulation.

III. Performance Characterization

To further improve the performance of the device, we investigated the effect of phase difference and amplitude ratio between two electric field components on the chirality of waveguide. The theoretical extinction ratio as a function of phase difference and amplitude ratio of longitude and transverse electric field components are shown in Fig. 5(a). The extinction ratio can be easily switched from peak to valley by just modulating the phase difference of 0.5π. This simple tuning method shows the feasibility and superiority in transverse spin dependent chiral waveguide research. Although it is theoretically predicted that the maximum extinction ratio should present in the condition of circular transverse spin, an appreciable deviation is found in the simulated extinction ratio map. Fig. 5(c) and (d) shows the phase difference and amplitude ratio dependence of the extinction ratio respectively. The black curves are marked in Fig. 5(a) by orthogonal black dash lines meet at the peak of extinction ratio, while the red curves corresponding to the red dashed lines meet at the position with circular transverse spin. The maximum extinction ratio of the chiral waveguide can reach up to 42 dB in our simulation when the phase difference and amplitude ratio are set to $[\varphi_{Ez\text{-}Ex}, |\boldsymbol{E}_z|/|\boldsymbol{E}_x|] = [0.34\pi, 0.66]$, which is distinctively deviated from circularly transvers spin ($[\varphi_{Ez\text{-}Ex}, |\boldsymbol{E}_z|/|\boldsymbol{E}_x|] = [0.5\pi, 1]$). To investigate the underlying physical mechanism of

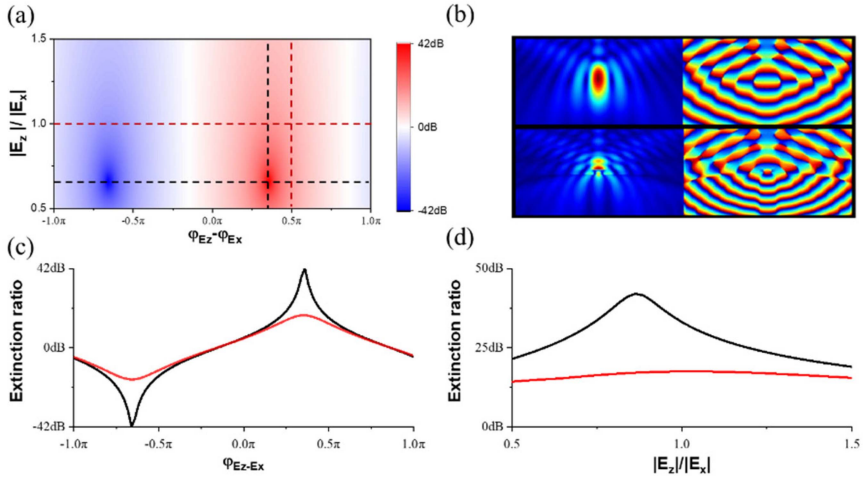

Fig. 5. The optimization process of the directionality of the designed chiral device. (a) The map of extinction ratio as a function of phase difference and amplitude ratio of two beams. (b) The amplitude and phase distribution of tight focused linearly polarized Gaussian beam. upside: light filed without the waveguide and substrate, downside: incident light field with the waveguide and substrate. (c) The extinction ratio as a function of the phase difference of two electric components on focal plane when the amplitude ratio $|\boldsymbol{E}_z|/|\boldsymbol{E}_x|$ equals to 0.66 (black curve) and 1 (red curve) respectively. (d) The extinction ratio as a function of the amplitude ratio factor of two electric components on focal plane when the phase difference is set to o.34π (black curve) and 0.5π (red curve) respectively.

the deviation, the phase and amplitude distribution of generated light field with transverse spin are simulated.

The images in Fig. 5(b) compared the amplitude and phase distribution of $\boldsymbol{E}_z$ component for tightly focused radially polarized beam with and without considering the scattering of the waveguide respectively. It is clear that the phase and amplitude distribution of the incident light field can be modified enormously by scattering of waveguide and the reflection of substrate. The initial phase difference and the amplitude ratio at the center of focus modulated from $[\varphi_{Ez\text{-}Ex}, |\boldsymbol{E}_z|/|\boldsymbol{E}_x|] = [0.5\pi,1]$ to $[\varphi_{Ez\text{-}Ex}, |\boldsymbol{E}_z|/|\boldsymbol{E}_x|] = [0.68\pi,1.4]$. The scattering of waveguide causes a phase shift of 0.18π and amplitude ratio Enhancement of 1.4. To compensate the light field modulation induced by the scattering of waveguide, the initial phase difference and amplitude ratio of incident light field should be set to [0.5π-0.18π,1/1.4], which equals to [0.32π,0.71], respectively. The residual deviation of phase and amplitude ratio from the peak of extinction ratio shown is Fig. 5(a) becomes relatively small ($\Delta\varphi = 0.02\pi$, $\Delta|\boldsymbol{E}_z|/|\boldsymbol{E}_x| = $-0.05) after compensation. The small residual deviation after the compensation may be induced from the coupling efficiency difference of gold nanoparticle for $\boldsymbol{E}_z$ and $\boldsymbol{E}_x$ components of light field, which can be completely eliminated by simply tuning the phase difference and amplitude ratio of two incident beams.

As the chirality of the spin dependent device originate from the symmetry-breaking of light field, rather than the geometry of the coupling antenna, the proposed chiral device is intrinsically insensitive to the wavelength of incident light. We characterized the broadband performance of the design chiral coupler by sweeping the wavelength of incident light in the simulations. By varying the wavelength of incident light from 475 nm to 875 nm, the extinction ratio as a function of wavelength is calculated from the simulation results and shown in Fig. 6(a). The minimum extinction ratio in the wavelength range from 500 nm to 875 nm is 36.2 dB, which is 1 to 2 orders of magnitude

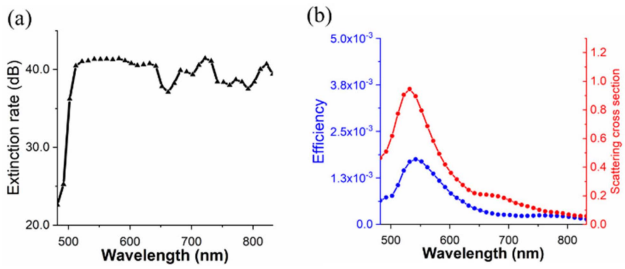

Fig. 6. The broadband performance of the chiral waveguide based on SOI. (a) The extinction ratio as function of the wavelength of incident light. (b) The coupling efficiency and normalized scattering cross section of the nano-antenna as function of the wavelength of incident light.

higher than the transverse spin dependent chiral device of same type reported in former works [11], [13], [26]. It should be noted that there is a sharp decrease of the chirality when the wavelength of incident light is shorter than 500 nm from Fig. 6(a). The decrease of chirality may result from the multimode excitation of the waveguide at shorter wavelength. For multimode excitation, the energy flow is no longer confined to the x direction in the waveguide, which will destroy the simple spin-direction bounding relation for the evanescent wave of single mode waveguide. The coupling efficiency and scattering cross section of the gold nanoparticle with diameter of 90 nm as function of wavelength of incident light are calculated by FDTD and shown in Fig. 5(b). It can be clearly seen that the coupling efficiency is directly dependent to the scattering cross section of the antenna, which will decrease as the wavelength of incident light increases. The positions of peaks of coupling efficiency and the scattering cross correspond to wavelength of 535 nm and 545 nm respectively, which ensures high coupling efficiency of the proposed chiral device at the designed wavelength of 532 nm. As the background noise is unavoidable for real word experiment, the chirality of the proposed device is associated with the coupling efficiency and

will decrease due to the degradation of coupling efficiency. The upper and lower limits of the operating bandwidth of the device are only determined by the number of eigenmodes of waveguide and the scattering cross-section of the antenna respectively. Therefore, the device proposed above can be applied to the infrared band by simply modifying the material and size of the waveguide and scatterer without redesigning the structure of the device.

IV. Conclusion

We have theoretically demonstrated a novel and configurable method to generate light field with transverse spin and numerically demonstrate its application in spin-dependent chiral nanophotonic waveguide. The key of this method is generating independent longitude and transverse electric field components in the focal volume by vector beam interference. The spin density of transverse spin in focal region is calculated using Richard-Wolf vectorial diffraction theory. A spherical valid volume of free-space light field with diameter of 250 nm in the focal volume has uniform a spin density above 0.85. A gold particle with diameter of 90 nm was utilized as antenna and placed in the valid volume to couple light into guided mode of a single mode Si_3N_4waveguide. The propagating direction of guided mode in the waveguide was controlled by tuning the handedness of transverse spin. Ultrahigh extinction ratio up to 42 dB was demonstrated numerically at wavelength of 532 nm after compensation of scattered field of waveguide. The underlying physical mechanism of phase difference and amplitude ratio deviation was studied via scattered field analysis. Our method has proven to be convenient for compensation of the deviation induced by the scattering of waveguide. The broadband performance of the chiral waveguide was also studied by varying the wavelength of incident light from 475 to 875 nm. Excellent broadband performance of the chirality for the designed transverse spin-dependent device was proven. The designed device process high extinction ratio above 36.2 dB in a fairly large wavelength range from 500 nm to 875 nm. The proposed configurable spin orbital coupling method in nanophotonic waveguide will find important applications in nanoscale optical router, quantum information processing, field mapping and novel spin controlled photonic devices.

References

[1] R. A. Beth, "Mechanical detection and measurement of the angular momentum of light," *Phys. Rev.*, vol. 50, no. 2, 1936, Art. no. 115.

[2] A. T. O'Neil et al., "Intrinsic and extrinsic nature of the orbital angular momentum of a light beam," *Phys. Rev. Lett.*, vol. 88, no. 5, 2002, Art. no. 053601.

[3] A. M. Yao and M. J. Padgett, "Orbital angular momentum: Origins, behavior and applications," *Adv. Opt. Photon.*, vol. 3, no. 2, pp. 161–204, 2011.

[4] M. V. Berry, "Paraxial beams of spinning light," *Proc. SPIE*, vol. 3487, pp. 6–11, 1998.

[5] J. H. Poynting, "The wave motion of a revolving shaft, and a suggestion as to the angular momentum in a beam of circularly polarised light," *Proc. Roy. Soc. London. Ser. A, Containing Papers a Math. Phys. Character*, vol. 82, no. 557, pp. 560–567, 1909.

[6] S. Asano and M. Sato, "Light scattering by randomly oriented spheroidal particles," *Appl. Opt.*, vol. 19, no. 6, pp. 962–974, 1980.

[7] K. Y. Bliokh et al., "Geometrodynamics of spinning light," *Nature Photon.*, vol. 2, no. 12, pp. 748–753, 2008.

[8] G. Molina-Terriza, J. P. Torres, and L. Torner, "Twisted photons," *Nature Phys.*, vol. 3, no. 5, pp. 305–310, 2007.

[9] K. Y. Bliokh et al., "Spin–orbit interactions of light," *Nature Photon.*, vol. 9, no. 12, pp. 796–808, 2015.

[10] C. P. Jisha and A. Alberucci, "Spin-orbit interactions in optically active materials," *Opt. Lett.*, vol. 42, no. 3, pp. 419–422, 2017.

[11] Y. Lefier and T. Grosjean, "Unidirectional sub-diffraction waveguiding based on optical spin–orbit coupling in subwavelength plasmonic waveguides," *Opt. Lett.*, vol. 40, no. 12, pp. 2890–2893, 2015.

[12] M. Neugebauer et al., "Polarization tailored light driven directional optical nanobeacon," *Nano Lett.*, vol. 14, no. 5, pp. 2546–2551, 2014.

[13] D. O'Connor et al., "Spin–orbit coupling in surface plasmon scattering by nanostructures," *Nature Commun.*, vol. 5, 2014, Art. no. 5327.

[14] D. Pan et al., "Strong spin-orbit interaction of light in plasmonic nanostructures and nanocircuits," *Phys. Rev. Lett.*, vol. 117, no. 16, 2016, Art. no. 166803.

[15] Z. Shao et al., "Spin-orbit interaction of light induced by transverse spin angular momentum engineering," *Nature Commun.*, vol. 9, no. 1, 2018, Art. no. 926.

[16] T. Van Mechelen and Z. Jacob, "Universal spin-momentum locking of evanescent waves," *Optica*, vol. 3, no. 2, pp. 118–126, 2016.

[17] A. P. Yang et al., "Optical transverse spin coupling through a plasmonic nanoparticle for particle-identification and field-mapping," *Nanoscale*, vol. 10, no. 19, pp. 9286–9291, 2018.

[18] K. Y. Bliokh and F. Nori, "Transverse spin of a surface polariton," *Phys. Rev. A*, vol. 85, no. 6, 2012, Art. no. 061801.

[19] M. Neugebauer et al., "Measuring the transverse spin density of light," *Phys. Rev. Lett.*, vol. 114, no. 6, 2015, Art. no. 063901.

[20] W. Zhu et al., "Transverse spin angular momentum of tightly focused full poincare beams," *Opt. Exp.*, vol. 23, no. 26, pp. 34029–34041, 2015.

[21] K. Y. Bliokh, A. Y. Bekshaev, and F. Nori, "Extraordinary momentum and spin in evanescent waves," *Nature Commun.*, vol. 5, no. 1, pp. 1–8, 2014.

[22] A. Aiello and J. P. Woerdman, "Role of beam propagation in Goos–Hänchen and Imbert–Fedorov shifts," *Opt. Lett.*, vol. 33, no. 13, pp. 1437–1439, 2008.

[23] Y. Gorodetski et al., "Weak measurements of light chirality with a plasmonic slit," *Phys. Rev. Lett.*, vol. 109, no. 1, 2012, Art. no. 013901.

[24] M. Onoda, S. Murakami, and N. Nagaosa, "Hall effect of light," *Phys. Rev. Lett.*, vol. 93, no. 8, 2004, Art. no. 083901.

[25] D. O'Connor et al., "Spin–orbit coupling in surface plasmon scattering by nanostructures," *Nature Commun.*, vol. 5, no. 1, 2014, Art. no. 5327.

[26] J. Petersen, J. Volz, and A. Rauschenbeutel, "Chiral nanophotonic waveguide interface based on spin-orbit interaction of light," *Science*, vol. 346, no. 6205, pp. 67–71, 2014.

[27] F. J. Rodríguez-Fortuño et al., "Near-field interference for the unidirectional excitation of electromagnetic guided modes," *Science*, vol. 340, no. 6130, pp. 328–330, 2013.

[28] S. Clément et al., "Nanophotonic optical isolator controlled by the internal state of cold atoms," *Phys. Rev. X*, vol. 5, no. 5, 2002, Art. no. 041036.

[29] P. E. Landreman and M. L. Brongersma, "Deep-subwavelength semiconductor nanowire surface plasmon polariton couplers," *Nano Lett.*, vol. 14, no. 2, pp. 429–434, 2014.

[30] A. E. Miroshnichenko and Y. S. Kivshar, "Polarization traffic control for surface plasmons," *Science*, vol. 340, no. 6130, pp. 283–284, 2013.

[31] J. Chen et al., "Experimental generation of complex optical fields for diffraction limited optical focus with purely transverse spin angular momentum," *Opt. Exp.*, vol. 25, no. 8, pp. 8966–8974, 2017.

[32] J. Chen et al., "Tightly focused optical field with controllable photonic spin orientation," *Opt. Exp.*, vol. 25, no. 16, pp. 19517–19528, 2017.

[33] W. Han et al., "Vectorial optical field generator for the creation of arbitrarily complex fields," *Opt. Exp.*, vol. 21, no. 18, pp. 20692–20706, 2013.

[34] C. Wan, Y. Yu, and Q. Zhan, "Diffraction-limited near-spherical focal spot with controllable arbitrary polarization using single objective lens," *Opt. Exp.*, vol. 26, no. 21, pp. 27109–27117, 2018.

[35] S. Zhang et al., "Fully controlled photonic spin in highly confined optical field," *Opt. Exp.*, vol. 27, no. 23, pp. 33621–33633, 2019.

[36] E. Collett, *Field Guide to Polarization*. Bellingham, WA, USA: SPIE, 2005.

[37] Y. Wang, E. W. Plummer, and K. Kempa, "Foundations of plasmonics," *Adv. Phys.*, vol. 60, no. 5, pp. 799–898, 2011.